Available online at www.sciencedirect.com
SCIENCE DIRECT®
Journal of Power Sources 138 (2004) 262–270
JOURNAL OF POWER SOURCES
www.elsevier.com/locate/jpowsour

# Electrochemical performance of $Al_2O_3$-coated Fe doped $LiCoVO_4$

N. Van Landschoot[a,*], E.M. Kelder[a], P.J. Kooyman[a], C. Kwakernaak[b], J. Schoonman[a]

[a] *Delft Institute for Sustainable Energy, Delft University of Technology, Laboratory for Inorganic Chemistry, Julianalaan 136, 2628 BL Delft, The Netherlands*
[b] *Laboratory for Material Science, Delft University of Technology, Rotterdamseweg 137, 2628 AL Delft, The Netherlands*

Received 28 January 2004; received in revised form 6 June 2004; accepted 21 June 2004
Available online 13 August 2004

**Abstract**

$Al_2O_3$-coated $LiCo_{0.94}Fe_{0.06}VO_4$ powders with improved electrochemical cycleability have been synthesized. The morphology and structure of the coating have been characterized with SEM, HR-TEM and XPS. It was found that the $Al_2O_3$ coating was amorphous and that the particles were not completely coated, approximately 30–40% of the surface was covered. The $Al_2O_3$ coating had an average thickness of 10 nm. Cyclic voltammetry measurements versus $Li/Li^+$ showed that the $Al_2O_3$-coated $LiCo_{0.94}Fe_{0.06}VO_4$ sintered at 600 °C showed the best capacity retention and the cycle tests revealed that the materials still possess a discharge capacity of 76 mA h $g^{-1}$, even after 80 cycles. The improved cycling performance is attributed to the ability of the $Al_2O_3$ layer to neutralize the HF component in the liquid electrolyte.


*Keywords:* $LiCoVO_4$; Surface modification; $Al_2O_3$; Li-ion batteries.

## 1. Introduction

In recent years, the demand for power sources with high-energy density has increased substantially due to the development and popularity of portable electronic devices, such as digital cameras, cellular phones, and electronic notebooks. The use of high-voltages materials is one way to achieve high-energy densities in batteries. Currently, three high-voltage cathode materials are commercially available, i.e., $LiNiO_2$, $LiCoO_2$, and $LiMn_2O_4$. Among the several new cathode materials under development, $LiMVO_4$ (M = Co, Ni) of the inverse spinel family proposed by Fey et al. [1–3] appears particularly interesting due to the higher voltage versus metallic Li compared to the commercially available cathode materials. The spinel phase materials are of extreme interest as the cathode active materials for their high-energy density. Most of the high-voltage (>4.5 V) cathodes have the spinel structure with the general formula $Li_{1-x}Mn_{2-y}M_yO_4$ (M = Cr, Fe, Co, Ni, and Cu) [4–12]. The voltage and structural charge and discharge voltage in the 5 V region depend on the transition metal ion M and the amount of cation substitution in $Li_{1-x}Mn_{2-y}M_yO_4$. As a result, the high-voltage (>4.5 V) capacity of these manganese-based $Li_{1-x}Mn_{2-y}M_yO_4$ cathodes has generally been attributed to the other transition metal ion redox couples $Fe^{3+/4+}$, $Ni^{2+/3+/4+}$, $Cu^{2+/3+}$.

Fey et al. [1–3] showed that the major drawback of these materials is the low electronic conductivity. In earlier papers, we showed that by doping $LiCoVO_4$ with Cu, Cr, and Fe, the electronic conductivity as well as the electrochemical performance were improved [13,14]. Despite the enhanced initial charge capacity, i.e. 110 mA h $g^{-1}$, the capacity fading is still relatively high. Capacity fading during charge and discharge is a well-known problem for intercalation materials. Several factors have been proposed to contribute to the fading, such as (i) electrolyte degradation due to electrolyte instability at higher voltages (<4.5 V), (ii) structural instability, or (iii) 3d metal ion dissolution due to HF generation induced by (a) temperature enhanced electrolyte degradation, (b) undesired-chemical reactions occurring at the solid/electrolyte interface or, (c) water contamination ($LiPF_6 \rightleftarrows LiF + PF_5$; $PF_5 + H_2O \rightleftarrows 2HF + POF_3$). In the

* Corresponding author. Tel.: +31 15 2785 536; fax: +31 15 2788047.
*E-mail address:* n.vanlandschoot@tnw.tudelft.nl (N.V. Landschoot).

0378-7753/$ – see front matter © 2004 Elsevier B.V. All rights reserved.
doi:10.1016/j.jpowsour.2004.06.046

$LiMn_2O_4$ spinel, the capacity fading was a result of Mn diffusion and dissolution into the electrolyte due to HF and a disproportionation reaction at the surface [15,16]. Not only in spinel-based materials but also in layered structures, such as $LiCoO_2$, the fading is often related to the dissolution of 3d metal ions. Based on the fact that Mn dissolution occurs at the interface of $LiMn_2O_4$ and the electrolyte, it is thought that a similar process occurs with Co and/or V in $LiCoVO_4$. To date, many research groups are investigating the prevention of dissolution of transition metal ions, using different surface modifications. One of these surface modifications is the coating of the particle with a dense and uniform coating. Park et al. [17] used a $LiCoO_2$ coating on $LiMn_2O_4$ to improve the rate of capability. The $LiMn_2O_4$ particle was covered with small particles of $LiCoO_2$ using a wet chemical process. An increase of the rate capability was observed. Sun et al. [18] used ZnO on $LiNi_{0.5}Mn_{1.5}O_4$, and found an improved cycling behaviour at 5 V due to the reduced reactivity of HF with the ZnO interface, compared to that of the $LiNi_{0.5}Mn_{1.5}O_4$ interface. Liu et al. [19] used an amorphous-$Al_2O_3$ coating on $LiCoO_2$. The coating was deposited on the particles using a wet chemical method. The improved cycleability was attributed to this amorphous layer, which prevented Co dissolution. All coatings reported so far were deposited on the particles using a wet chemical process.

$Al_2O_3$ is a technologically important material due to its excellent dielectric properties, good adhesion to many surfaces, and thermal and chemical stability. These properties make $Al_2O_3$ attractive in silicon microelectronics and as a protective coating. Applications for $Al_2O_3$ films are also being investigated in a variety of other areas including solar energy devices. In these devices, $Al_2O_3$ is often used as a diffusion barrier [20]. One of the properties of $Al_2O_3$ is that the material is an electronic insulator. Applying a coating of $Al_2O_3$ on $LiCoVO_4$ lowers the ionic and electronic conductivity. However, when the film thickness is reduced to values $\leq$4 nm, a direct tunnelling of electrons has been reported by Groner et al. [21]. This direct tunnelling can be identified as Fowler–Nordheim (FN) tunnelling [21]. The authors also observed this direct tunnelling for layers with a thickness of 12.2 nm but at higher applied potentials, i.e., 4 V.

In this paper, Fe-doped $LiCoVO_4$ is coated with $Al_2O_3$ using a wet chemical process and the influence of this coating on the structural and electrochemical properties are being discussed.

## 2. Experimental

$LiCo_{0.94}Fe_{0.06}VO_4$ was prepared via the citric-acid complex method. The citric-acid complex method is a well-known method for the preparation of sub-micron based particles [22]. Appropriate amounts of $Li_2CO_3$ (>99%, Baker Analyzed), $CoCO_3{\cdot}H_2O$ (>99%, Merck), $NH_4VO_3$ (>98%, Acros Organics), and $FeCl_2{\cdot}4H_2O$ (>98%, Acros Organics,) were mixed together in 100 ml of distilled water under constant-magnetic stirring at 80 °C. To the solution, 100 ml of a 0.3 M citric acid solution was slowly added. The solution was then held at 100 °C for 1 h forming a gel. Subsequently, the gel was heated at 120 °C in a vacuum furnace for 3 h. The obtained precursor was fired at 500 °C in air for 2 h and the obtained powder was ball milled afterwards. This procedure was repeated ones here after.

The $LiCo_{0.94}Fe_{0.06}VO_4$ particles were coated with $Al_2O_3$ via a wet chemical process. The powder (0.5 g) was dispersed in a 0.1 M solution of $NaHCO_3$ (99%, Aldrich) under constant-magnetic stirring for 2 h in order to disperse the particles. Dropwise, 5 ml of a 0.1 M solution of $Al(NO_3)_3{\cdot}9H_2O$ (>98%, Aldrich) was added to the dispersion. The suspension was stirred for 2 h at room temperature. The following reactions occur [10]:

$$HCO_3^- + H_2O \rightarrow H_2CO_3 + OH^-$$

$$H_2CO_3 \rightarrow H_2O + CO_2 \uparrow$$

$$Al_3^+ + 3OH^- \rightarrow Al(OH)_3 \downarrow$$

The suspension was filtered over a Buchner funnel and, subsequently, washed with distilled water. The powder was dried overnight in a vacuum furnace at 120 °C and sintered at different temperatures, i.e., 200 °C, 400 °C, 600 °C, and 800 °C for 2 h. The coating procedure was repeated in order to obtain a more completely coated particle.

Electrodes were made using a doctor–blade technique on a 12 μm-thick aluminium foil. The electrodes contain 85 wt.% of active material, 6 wt.% of carbon black (MMM Carbon), and 9 wt.% of PVDF (Solef). From the foils, Ø15-mm discs were punched out. The cells were assembled in a helium-filled glove box with metallic Li as the anode. 1 M $LiPF_6$ dissolved in EC/DMC 1:2 (Mitsubishi Chem.) was used as the electrolyte with Solupor® (DSM Solutech) as separator. Electrochemical characterizations were performed using CR2320 coin type cells. The batteries were cycled between 3.0 V and 4.5 V for 10 cycles using a MACCOR battery tester. The charge and discharge currents were 0.2 mA $cm^{-2}$. This corresponds to a C/10-rate. For the cyclic voltammetry measurements an Autolabs PGSTAT12 potentiostat/galvanostat was used with a scan speed of 0.1 mV $s^{-1}$ between 3.0 V and 4.5 V.

TEM measurements were performed using a Philips CM30T electron microscope with a $LaB_6$ filament as the source of electrons operated at 300 kV. Samples were mounted on Quantifoil® carbon polymer supported on a copper grid by placing a few droplets of a suspension of ground sample in ethanol on the grid. The grid was dried at ambient conditions. Elemental composition was obtained by energy dispersive analysis of X-rays (EDX) performed through a LINK–EDX system. For all samples, TEM measurements were taken from the coated-pristine powder and the cycled powder.

X-ray photon spectroscopy (XPS) measurements were performed on the pure and $Al_2O_3$-coated powder in a PHI

5400 ESCA instrument of Physical Electronics Corporation with a 400 W non-monochromatized Mg Kα X-ray radiation source. During measurements, the background vacuum was $2 \times 10^{-7}$ Pa or better. The photo-electron spectra were recorded with a spherical capacitor analyzer set at constant pass energy of 71.55 eV and with a step size of 0.25 eV. The emitted photo electrons were detected at 45° with respect to the surface normal to the specimen. The decomposition of the photo-electron peaks was obtained as follows. Firstly, the satellites were removed from the spectrum. Secondly, the measured spectrum was corrected for electrostatical charging by shifting the entire spectrum using the C1s peak to the adopted value of the binding energy of 284.80 eV. The spectra was fitted with Gauss–Lorentz profiles using Shirley backgrounds.

For the conductivity measurements, the coated and pristine $LiCo_{0.94}Fe_{0.06}VO_4$ powders were pressed into pellets with a diameter of 10 mm and an average thickness of 1 mm at a pressure of 1500 kg cm$^{-2}$. The pellets were then sintered at 500 °C for 16 h in air. After the sintering step, the pellet surfaces were sputtered with gold for 10 min on both sides using a sputter coater (Edwards). The electrical conductivity measurements were performed using a Schlumberger Solatron 1260 frequency response analyzer. The applied ac voltage was 10 mV peak–peak in the frequency range 1–10 MHz. The temperature range was between 50 °C and 160 °C.

## 3. Results and discussion

In order to investigate the influence of the dissolution of 3d metals, due to the HF attack, on the electrochemical properties of the inverse spinel, the uncoated $LiCo_{0.94}Fe_{0.06}VO_4$ was tested versus metallic Li with a pulse charge test. The cell was charged for 15 min at a constant current of 0.02 mA h cm$^{-2}$, which corresponds to a C/100, followed by a rest step of 5 min, as shown in Fig. 1. The cell was cycled up to 4.6 V. At voltages beyond 4.3 V, an increase in the voltage drop, i.e., polarization, during rest is observed. This voltage drop increases from 20 mV up to 120 mV at 4.6 V. At 4.3 V 0.55 $Li^+$ has been extracted approximately from the inverse spinel. From $LiCoO_2$, it is known that cobalt dissolution [23] already occurs at slightly lower voltages, namely 4.1 V versus Li/$Li^+$. The dissolution of Mn from the spinel $LiMn_2O_4$ occurs in the charged state at >4.1 V versus Li/$Li^+$ [24]. To investigate the increase of this voltage drop on the dissolution of the 3d metals as a function of the lattice parameter, nine electrochemical cells were made, i.e., based on $Li_xCo_{0.94}Fe_{0.06}VO_4$. The cells were charged with $x$ ranging from 1 down to 0.2 with intermediate steps of 0.1. The cells were disassembled, subsequently, in a glove box and of each cell the electrolyte was analyzed for the presence of either cobalt and/or vanadium, using atomic absorption spectroscopy (AAS). The de-lithiated active materials were studied with X-ray diffraction in order to characterize the structural changes. Results are presented in Fig. 2. Fig. 2 shows the nominal composition of $Li_xCo_{0.94}Fe_{0.06}VO_4$ versus the obtained lattice parameter and as a function of $x$ and of the amount of dissolved cobalt and vanadium, i.e., not corrected yet for the amount of dissolved cobalt and vanadium. From the X-ray diffraction patterns it was concluded that no new phases appeared and that the inverse spinel structure remained intact and, therefore, the patterns are not shown here. Up to $Li_{0.6}Co_{0.94}Fe_{0.06}VO_4$, almost no

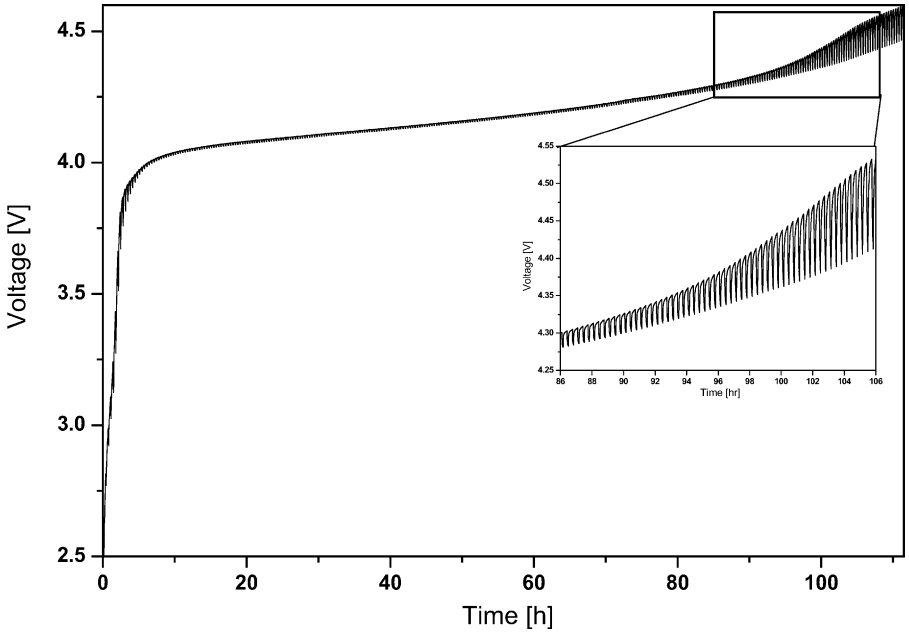


Fig. 1. Charge pulse test of $LiCo_{0.94}Fe_{0.06}VO_4$ vs. Li/$Li^+$, $I_{charge}$ = 0.02 mA h cm$^{-2}$ applied for 15 min and subsequently 5 min rest. The cell was cycled up to 4.6 V.

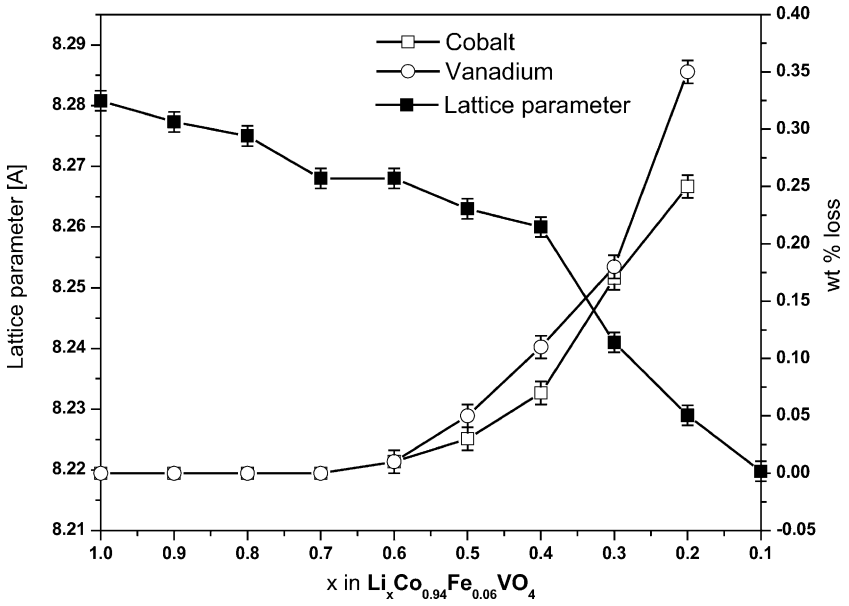


Fig. 2. The relationship of de-lithiated $Li_xCo_{0.94}Fe_{0.06}VO_4$ powders vs. the lattice parameter of $Li_xCo_{0.94}Fe_{0.06}VO_4$ and the amount of dissolved cobalt and vanadium in the electrolyte.

traces of cobalt and vanadium were observed in the electrolyte and there is a linear change in the lattice parameter. Beyond $Li_{0.6}Co_{0.94}Fe_{0.06}VO_4$ an increase in the amount of cobalt and vanadium was found in the electrolyte, which caused a direct increase in polarization of the cell as presented in Fig. 1. A large decrease of the lattice parameter is observed beyond $Li_{0.4}Co_{0.94}Fe_{0.06}VO_4$, while at the same time the amount of dissolved vanadium and cobalt increased rapidly. The increase in the dissolution of the 3d metals beyond $Li_{0.4}Co_{0.94}Fe_{0.06}VO_4$ causes an increase in the polarization of the cell as shown in Fig. 1. From these results, it is plausible to conclude that there is a direct correlation between the increase in the polarization of the cell and the dissolution of the 3d metals. The dissolution of the 3d metals leads to an alteration of the active surface causing an increase in the impedance and increased irreversible charge capacity. To overcome the dissolution problem, which leads to an increase in the internal resistance and lowers the performance of the active materials, the active materials were coated with $Al_2O_3$.

Fig. 3 shows the morphologies of the pristine (a) and the coated (b) $LiCo_{0.94}Fe_{0.06}VO_4$. The coated powder was sintered at 500 °C for 2 h in air. The particle size is between 0.3 μm and 2.5 μm and some particles are clustered. The surfaces of the pristine and the coated powder are smooth and do not differ from one other as can be seen in Fig. 3 at this magnification. No differences in morphologies arising from the $Al_2O_3$ coating can be observed. Often this kind of coating technique reveals small particles covering the surface [18,19,25]. SEM pictures reveal a rather smooth layer of $Al_2O_3$, which is usually difficult to distinguish with SEM. Therefore, we used HR-TEM to differentiate between the particle and the coating. From the EDX analyses, as shown in Fig. 4, it was concluded that the coating was $Al_2O_3$. The EDX analysis shows a small signal for Al and more intense signals for Co, Fe and V. The Cu signal is from the grid and at this moment the origin of the Si signal is still unclear. Other EDX analyses on different coated samples did not show the Si signal. Fig. 5 shows HR-TEM images of the coated active material. The $Al_2O_3$ coating was found to be amorphous and not uniform in thickness. The images further reveal that not all the particles were coated and that the $Al_2O_3$ coating reached a maximum thickness of about 20 nm. From the TEM images it was estimated that approximately 30–40% of the surface was covered. In addition, the HR-TEM images also reveal some small or clustered particles of pure $Al_2O_3$ on the surface.

XPS was employed to study the surface composition of the $Al_2O_3$-coated material and to determine whether the coating had formed a solid-solution, e.g., $LiAlO_2$. The formation of this solid-solution at the interface of the particle and the coating is undesired. Although recently Sun et al. [26] showed that $LiAlO_2$ possesses good surface properties for $LiMn_2O_4$ at elevated temperatures. Fig. 6a shows the XPS spectra of the $Al_{2p}$ for coated material. The observed binding energy of the $Al_{2p}$ is 70.2 eV, which is slightly lower than reported data. Fig. 6b presents the $O_{1s}$ spectra of the pristine and coated material. The binding energy of $O_{1s}$ of the pristine material is 529.7 eV and this value does not change after the surface modification, although a shoulder does appear on the $O_{1s}$ peak. This shoulder, as indicated with an arrow in Fig. 6b, represents a binding energy of 531.9 eV, which corresponds to the $O_{1s}$ peak of $Al_2O_3$ [27]. The fitted $O_{1s}$ peak of $Al_2O_3$-coated $LiCo_{0.94}Fe_{0.06}VO_4$ is added to Fig. 6b and clearly shows two peaks. The fitted $O_{1s}$ peak revealed that the area distribution is 20% for $Al_2O_3$ and 80% for $LiCo_{0.94}Fe_{0.06}VO_4$. These

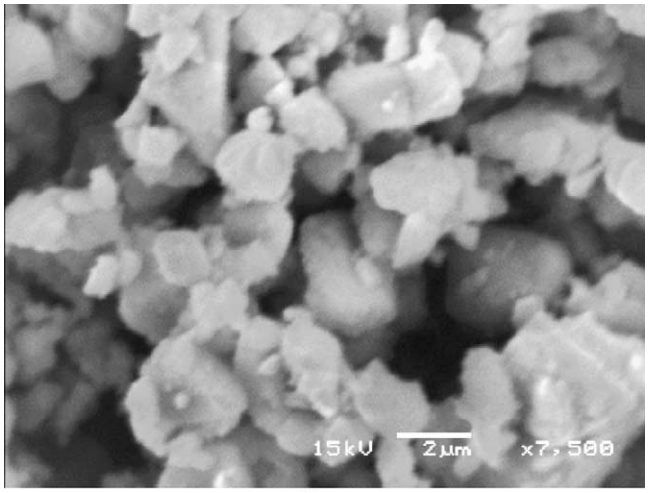


(a)

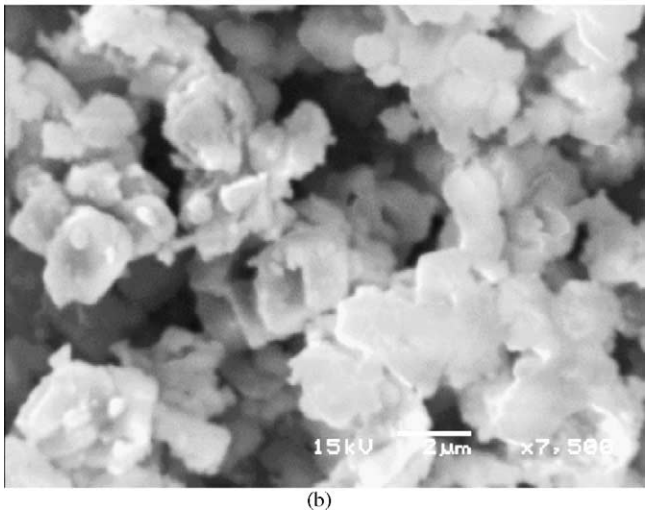


(b)

Fig. 3. (a) SEM image of $LiCo_{0.94}Fe_{0.06}VO_4$. (b) SEM image of $LiCo_{0.94}Fe_{0.06}VO_4$ coated with $Al_2O_3$.

values correspond to the HR-TEM observations. The binding energies for the $V_{2p1}$ and the $V_{2p3}$ as obtained from the spectra of the coated powder compared to the pristine powder reveal no changes in the binding energy values. The $Al_2O_3$ coating has no influence on the chemical state or on the binding energies of the different ions in the pristine material. Therefore, we conclude that no solid-solution, like $LiAlO_2$ has formed between the $Al_2O_3$ and $LiCo_{0.94}Fe_{0.06}VO_4$. These results are consistent with the TEM observations. A more detailed explanation of the XPS spectra of the pristine material will be discussed in the near future [28].

Cyclic voltammograms of the coated materials, sintered at different temperatures, are presented in Fig. 7(a–d). The capacity of the coated-active materials sintered at 200 °C and 400 °C as shown in Fig. 7a and b is still fading. In Fig. 7a a sharp-oxidation peak is observed during the second cycle. Such a sharp peak has also been observed before with other coated-active materials, even during the reverse scan. The nature of this oxidation peak is under investigation. Fig. 7d shows the cyclic voltammogram of the coated-active material sintered at 800 °C. This voltammogram clearly reveals a large capacity fading during the first four cycles and also that the polarization (voltage difference between the charge and discharge curves) increases dramatically with increasing cycle number, indicating a structural degradation of the $Al_2O_3$-coated $LiCo_{0.94}Fe_{0.06}VO_4$ electrode. This polarization effect was also present in the uncoated $LiCo_{0.94}Fe_{0.06}VO_4$, prepared via a solid-state reaction at 800 °C, as reported by Van Landschoot et al. [13]. The $Al_2O_3$ coating could be destroyed at this relative-high temperature, forming an Al-doped $LiCo_{0.94}Fe_{0.06}VO_4$ solid-solution. However, the XRD pattern did not indicate any difference between the coated powers sintered at 600 °C or at 800 °C. TEM measurements, not shown here, on this material annealed at 800 °C did reveal that the amount of amorphous $Al_2O_3$ was substantially

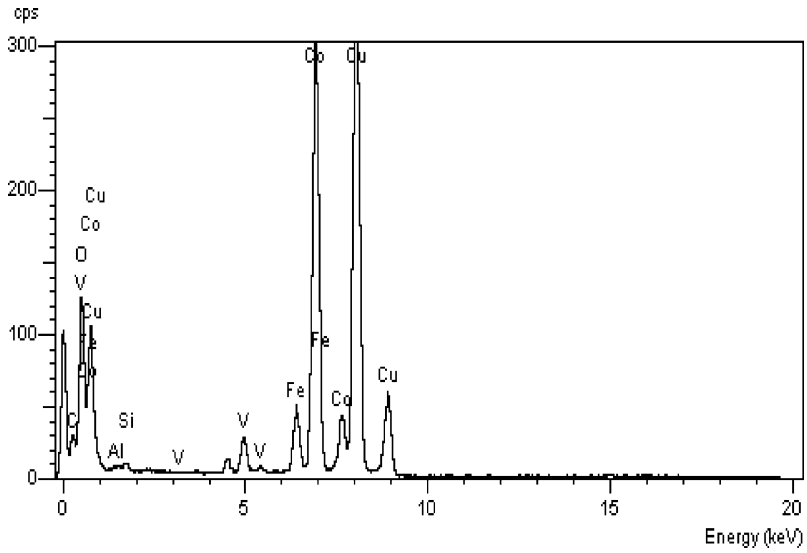


Fig. 4. EDX analysis of the $Al_2O_3$ layer. The Cu signal is due to the Cu-grid.

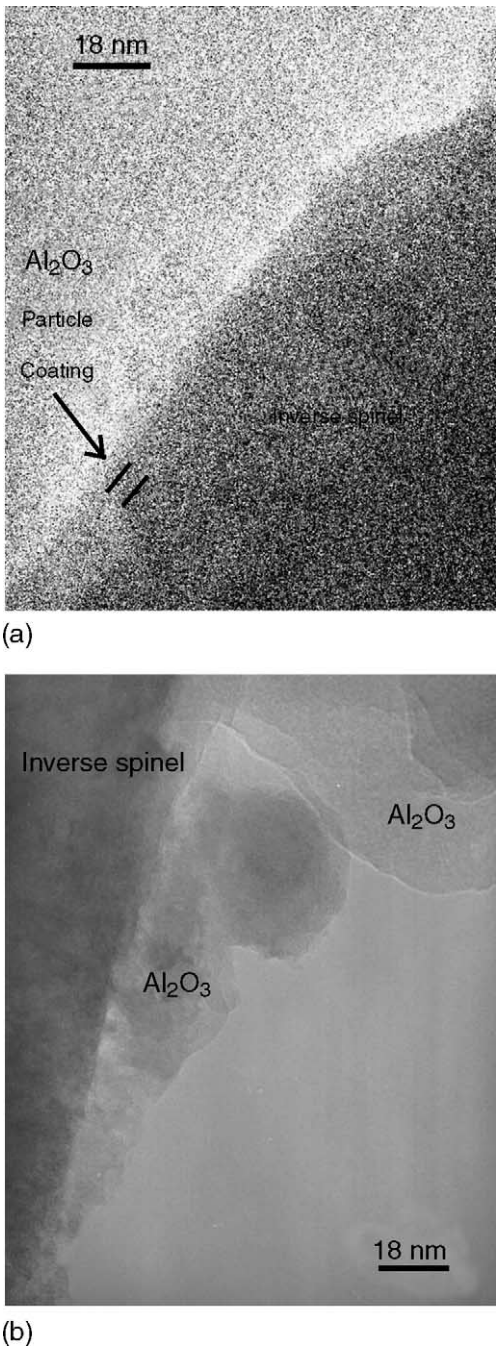


Fig. 5. (a) A HR-TEM image of $Al_2O_3$-coated $LiCo_{0.94}Fe_{0.06}VO_4$. (b) A HR-TEM image of $Al_2O_3$-coated $LiCo_{0.94}Fe_{0.06}VO_4$.

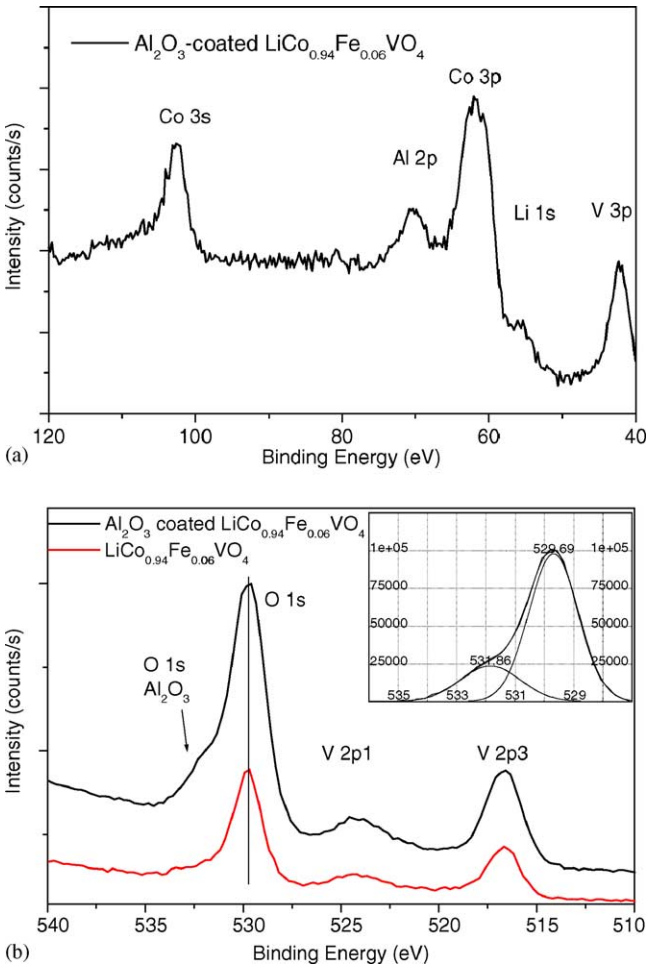


Fig. 6. (a) $Al_{2p}$ spectrum of the $Al_2O_3$-coated $LiCo_{0.94}Fe_{0.06}VO_4$. (b) $O_{1s}$ spectra of the pristine and $Al_2O_3$-coated $LiCo_{0.94}Fe_{0.06}VO_4$. The inset shows the fitted $O_{1s}$ spectra of $Al_2O_3$-coated $LiCo_{0.94}Fe_{0.06}VO_4$.

less compared to the materials synthesised at lower temperatures. On the TEM images we could not distinguish between the solid-solution and the bulk. The coated-active material sintered at 600 °C shows a very stable capacity retention even after four cycles. The polarization effect is very small compared to the coated materials sintered at 200 °C, 400 °C and, 800 °C. With the active material sintered at 600 °C, the most promising results were obtained. Liu et al. [19] also found that the optimal-sintering temperature in terms of stability and capacity retention was 600 °C for $Al_2O_3$ on $LiCoO_2$. Fig. 8 presents the charge and discharge curve of the coated and uncoated $LiCo_{0.94}Fe_{0.06}VO_4$. The cycling behaviour of the electrode shows clearly the impact of the $Al_2O_3$ coating in protecting the surface against HF attack. The uncoated $LiCo_{0.94}Fe_{0.06}VO_4$ has a discharge capacity of 37 mA h $g^{-1}$ after 16 cycles compared to 76 mA h $g^{-1}$ for the coated $LiCo_{0.94}Fe_{0.06}VO_4$ after 80 cycles. The minor fluctuations in the data are caused by fluctuations in temperature. Thackeray et al. [29] suggested that the improved cycleability of $ZrO_2$-coated $LiMn_2O_4$ was due to the negatively charged, amphoteric surface that scavenges the acidic HF species from the electrolyte. We are inclined to believe that this explanation is also valid for the $Al_2O_3$ coating, as $Al_2O_3$ behaves also amphoteric on our active material. However, the capacity fading of the coated $LiCo_{0.94}Fe_{0.06}VO_4$ is quite substantial, i.e., approximately 30 mA h $g^{-1}$ over the first five cycles, after which the capacity retention becomes quite stable. The HR-TEM images show that not all the particles were coated and that this is one of the main reasons why the capacity decrease is still substantial. In order to examine the influence of the $Al_2O_3$ coating on the amount of HF and the amount of dissolved

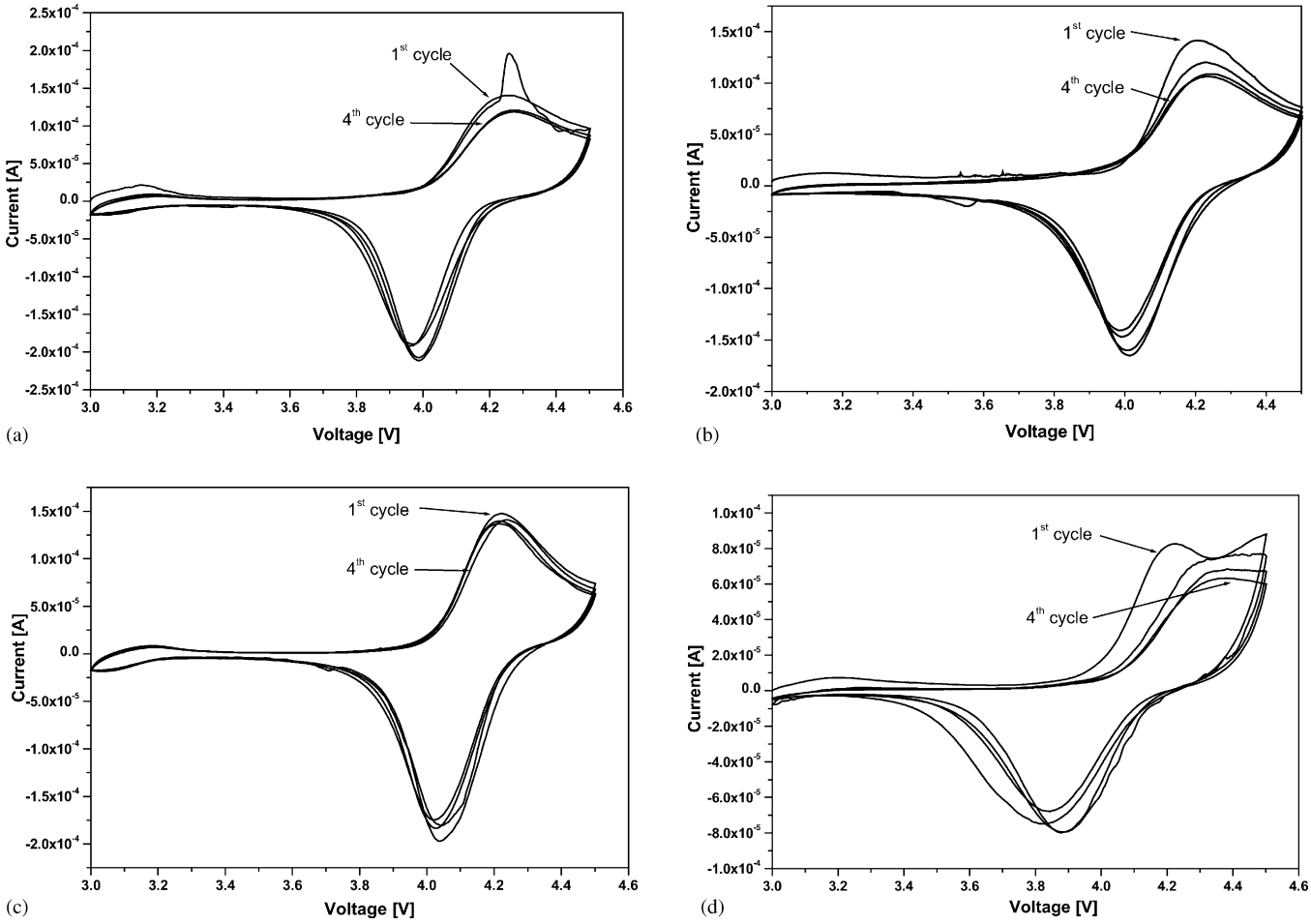


Fig. 7. Cyclic voltammogram of the first four cycles of the $Al_2O_3$-coated $LiCo_{0.94}Fe_{0.06}VO_4$ vs. metallic Li, sintered at different temperatures: (a) 200 °C; (b) 400 °C; (c) 600 °C; (d) 800 °C. The scan rate is 0.1 mV $s^{-1}$ between 3.0 V and 4.5 V.

3d metals, the coin cells with coated and uncoated electrodes were opened in the glove box and appropriate amounts of electrolyte were analyzed by atomic absorption spectroscopy (AAS). The results are shown in Table 1. The amount of HF in the electrolyte of the uncoated $LiCo_{0.94}Fe_{0.06}VO_4$ is substantially higher compared to the amount of HF in the electrolyte of the coated $LiCo_{0.94}Fe_{0.06}VO_4$. The substantial increase in the HF could be explained by the electrolyte degradation due to high cut off voltage of 4.5 V. The slightly lower increase of the HF amount is due to the $Al_2O_3$ coating, which also hinders the dissolution of the 3d metals in the electrolyte shown in Table 1. The amounts of cobalt and vanadium found in the electrolyte indicate that the $LiCo_{0.94}Fe_{0.06}VO_4$ particles were not fully coated as was already shown by the HR-TEM results in Fig. 2a and b. One of the fading mechanisms of $LiMn_2O_4$ is the migration of $Mn^{2+}$ ions to the anode. In order to investigate the migration of one of the dissolved cations, Co or V, a cycled cell was disassembled in the glove box and the Li metal electrode was examined with EDX. The EDX analysis showed no traces of the dissolved cations on the Li metal electrode.

ac-impedance spectroscopy measurements as a function of reciprocal temperature on the coated and pristine powders were conducted to investigate the influence of the $Al_2O_3$ coating on the electrical conductivity. The coated and pristine powders were pressed into pellets with a diameter of 10 mm and an average thickness of 1 mm at a

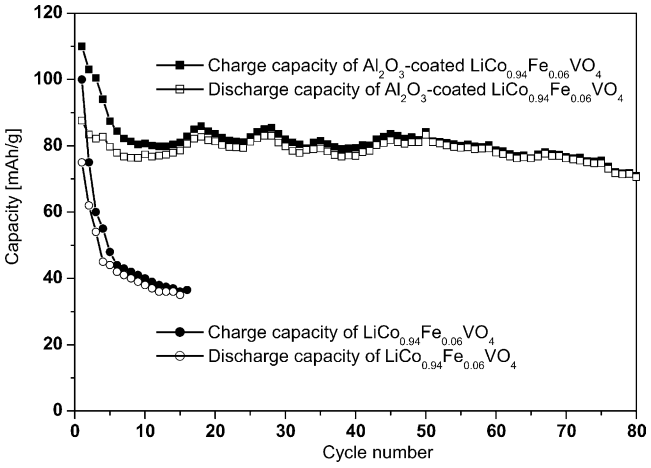


Fig. 8. Charge–discharge curves between 3.0 V and 4.5 V for pristine and $Al_2O_3$-coated $LiCo_{0.94}Fe_{0.06}VO_4$ sintered at 600 °C ($I_{charge}$ = 0.2 mA $cm^{-2}$, $I_{discharge}$ = 0.2 mA $cm^{-2}$). This corresponds to a C/10 rate.

Table 1
The electrolyte compositions from the cycled uncoated and $Al_2O_3$-coated $LiCo_{0.94}Fe_{0.06}VO_4$ analyzed with AAS

| | HF (ppm) | Co (wt.%) | V (wt.%) | Fe (wt.%) |
|---|---|---|---|---|
| Pristine electrolyte 1 M $LiPF_6$EC/DMC 1:2 | 18 | – | – | – |
| $LiCo_{0.94}Fe_{0.06}VO_4$ after 16 cycles | 45 | 1.1 | 2.3 | <0.01 |
| $Al_2O_3$ coated $LiCo_{0.94}Fe_{0.06}VO_4$ after 80 cycles | 30 | 0.45 | 0.87 | <0.01 |

pressure of 1500 kg cm$^{-2}$. The pellets were sintered subsequently at 500 °C for 16 h in air. After the sintering step, the pellets were sputtered with gold for 10 min on both sides. The applied voltage was 10 mV peak–peak in the frequency range 1 Hz–10 MHz. The temperature region was between 50 °C and 160 °C. Fig. 9 shows the impedance spectra of both pellets measured at 160 °C and the equivalent circuits are presented in the spectra. The sample dimensions have been used in the analyses of the measurements. Since $LiCo_{0.94}Fe_{0.06}VO_4$ is a mixed ionic and electronic conductor (MIEC), two parallel branches representing ionic and electronic conduction pathways are expected. The use of $Li^+$-ion blocking electrodes results in a dc conduction pathway for electrons and blocking behaviour for $Li^+$-ions under dc conditions [30]. The data can be fitted including a constant-phase element (CPE) to allow for depression of the arc. The difference between both equivalent circuits is the addition of an other branch representing grain polarization via a $R_{grain} - C_{grain}$ parallel branch representing the $Al_2O_3$ coating in series with $R_{bulk}$. The spectra recorded at higher temperatures revealed excellent fit results ($\chi^2$ = 6.8549E − 5 for the coated powder, and 7.1970E − 5 for the pristine powder). The CPE value for the pristine powder is around 0.65 and increases slightly with increasing temperatures. The CPE values for the coated powder are quite low, i.e., around 0.30 and decrease slightly. The low CPE value, being a result of the suppressed arcs, is caused by the $Al_2O_3$ coating. This phenomenon is also seen in composite materials [31]. Fig. 10 shows Arrhenius plots of the electrical conductivities of the pellets derived from $R_{bulk}$ and $R_{grain}$. The electrical conductivity, obtained from $R_{bulk}$, is similar ($10^{-7}$ S cm$^{-1}$ at 50 °C) for both cells. However, the total electrical conductivity for the coated powder is lower, as a result of the presence of the insulating $Al_2O_3$ layer. The activation energies for $R_{bulk}$ are 0.19 ± 0.02 eV for the pristine power and 0.22 ± 0.02 eV for the coated powder and are practically similar. This indicates that in pristine and coated powders a similar conduction mechanism occurs.

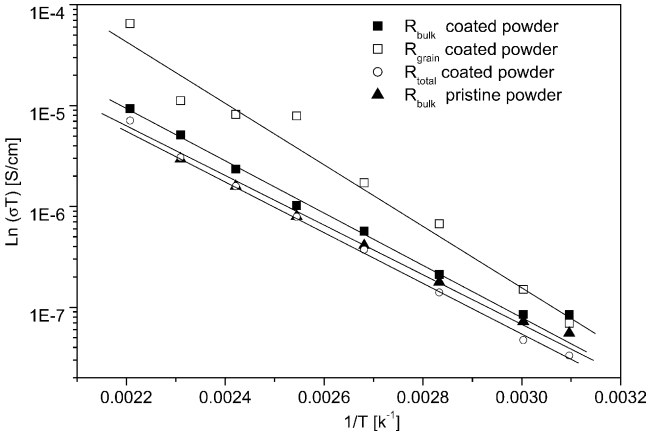


Fig. 10. Electrical conductivities in [S cm$^{-1}$] of the pristine and coated powders as a function of the reciprocal temperature.

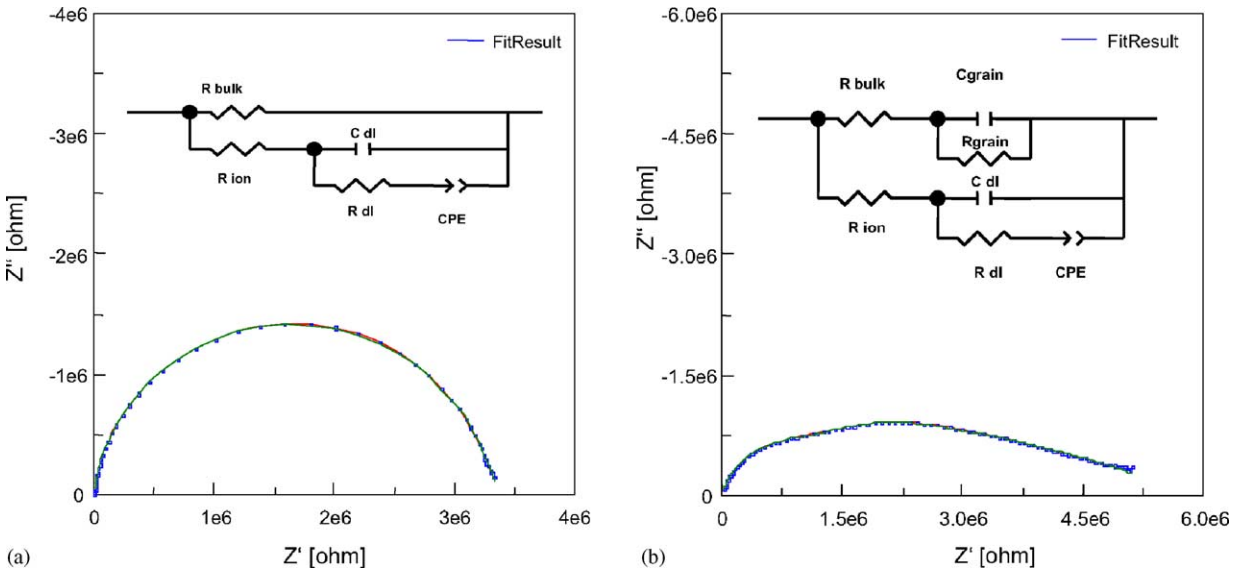


Fig. 9. ac-impedance spectroscopy spectra and fitted spectra of the cells: (a) Au//$LiCo_{0.94}Fe_{0.06}VO_4$//Au; (b) Au//coated $LiCo_{0.94}Fe_{0.06}VO_4$//Au; measured at 160 °C between 1Hz and 10 MHz. The sample geometry and thickness have been taken into account in the analyses of the measurements.

The present surface modification by $Al_2O_3$ of an electrochemically active particle is not favourable in terms of electronic conductivity. The decrease in the electronic conductivity is not favourable, especially, when these coated systems are to be used for high-power applications, unless the coating is uniform in thickness and thinner than 4 nm. For a coating thinner than 4 nm, a direct tunnelling of electrons through the coating is expected. On the other hand, not much is known of a $Li^+$ ion tunnelling through such a thin-$Al_2O_3$ structure, but is assumed to be difficult. It is favourable for the $Li^+$ ions to migrate through a surface modification that has the same crystal structure in order to overcome a structural mismatch.

## 4. Conclusions

A significant improvement in the capacity and cycling stability was achieved by partly coating $LiCo_{0.94}Fe_{0.06}VO_4$ with amorphous $Al_2O_3$ as concluded from XPS and TEM analyses. The particles were coated using a wet chemical technique. The improvement of the capacity was attributed to the ability of the $Al_2O_3$ layer to neutralize the HF component in the liquid electrolyte as a result of the reaction of residual $H_2O$ in the electrolyte or electrode with $LiPF_6$. The TEM images revealed that the particles were not completely coated but the surface modification does enhance the performance of $LiCo_{0.94}Fe_{0.06}VO_4$. The total electrical conductivity of the coated powder is lower, as a result of the presence of the insulating $Al_2O_3$ layer as observed in ac impedance spectroscopy measurements. The $LiCo_{0.94}Fe_{0.06}VO_4$ with an $Al_2O_3$-coating sintered at 600 °C gave the best results with a discharge capacity of 76 mA h $g^{-1}$ after 80 cycles. Coated $LiCo_{0.94}Fe_{0.06}VO_4$ sintered at 800 °C in air showed a decrease in the capacity retention due to the formation of an Al-doped $LiCo_{0.94}Fe_{0.06}VO_4$ solid-solution.

## Acknowledgements

Dr. G. Calis of DSM Solutech is gratefully acknowledged for providing the separator material.

## References

[1] G.T.K. Fey, K.S. Wang, S.M. Wang, J. Power Sources 68 (1997) 159.
[2] G.T.K. Fey, C. Wu, Pure Appl. Chem. 69 (1997) 2329.
[3] G.T.K. Fey, W. Li, J.R. Dahn, J. Electrochem. Soc. 141 (1994) 2279.
[4] M.M. Obrovac, Y. Gao, J.R. Dahn, Phys. Rev. B 57 (1998) 5728.
[5] C. Sigala, D. Guyomard, A. Verbaere, Y. Diffard, M. Tournoux, Solid State Ionics 81 (1995) 167.
[6] H. Kawai, M. Nagata, M. Tabuchi, H. Tukamoto, A.R. West, Chem. Mater. 10 (1998) 3266.
[7] H. Shigemura, H. Sakaebe, H. Kageyama, H. Kobayashi, A.R. West, R. Kanno, S. Morimoto, S. Nasu, M. Tabuchi, J. Electrochem. Soc. 148 (2001) A730.
[8] H. Kawai, M. Nagata, H. Tukamoto, H. Kageyama, A.R. West, Electrochim. Acta 45 (1999) 315.
[9] Y. Gao, K. Myrtle, M. Zhang, J.N. Reimers, J.R. Dahn, Phys. Rev. B 54 (1996) 16670.
[10] Q. Zhong, A. Banakdarpour, M. Zhang, Y. Gao, J.R. Dahn, J. Electrochem. Soc. 144 (1996) 205.
[11] Y. Ein-Eli, W.F. Howard Jr., J. Electrochem. Soc. 144 (1997) L205.
[12] Y. Ein-Eli, W.F. Howard Jr., S.H. Lu, S. Mukerjee, J. McBreen, J.T. Vaughey, M.M. Thackeray, J. Electrochem. Soc. 145 (1998) 1238.
[13] N. Van Landschoot, E.M. Kelder, J. Schoonman, J. Electrochem. Soc., submitted for publication.
[14] N. Van Landschoot, E.M. Kelder, J. Schoonman, Solid State Ionics 166 (2004) 307.
[15] A. Blyr, C. Sigala, G.G. Amatucci, D. Gyomard, J.-M. Tarascon, J. Electrochem. Soc. 145 (1998) 194.
[16] L.-F. Wang, C.-C. Ou, K.A. Striebel, J.-S. Chen, J. Electrochem. Soc. 150 (2003) A905–A911.
[17] S.-C. Park, Y.-S. Han, Y.-S. Kang, P.S. Lee, S. Ahn, H.-M. Lee, J.-Y. Lee, J. Electrochem. Soc. 148 (2001) A680.
[18] Y.-K. Sun, K.-J. Hong, J. Prakash, K. Amine, Electrochem. Com. 4 (2002) 344.
[19] L. Liu, Z. Wang, H. Li, L. Chen, X. Huang, Solid State Ionics 152-153 (2002) 341.
[20] X.-T. Zhang, I. Sutanto, T. Taguchi, K. Tokuhiro, Q. Meng, T.N. Rao, A. Fujishima, H. Watanabe, T. Nakamori, M. Uragami, Solar Energy Mater. Solar Cells 80 (3) (2003) 315.
[21] M.D. Groner, J.W. Elam, F.H. Fabreguette, S.M. George, Thin Solid Films 413 (2002) 186.
[22] R. Alcántara, P. Lavela, J.L. Tirado, R. Stoyanova, E. Kuzmanova, E. Zhecheva, Chem. Mater. 9 (10) (1997) 2145.
[23] G.G. Amatucci, J.M. Tarascon, L.C. Klein, Solid State Ionics 83 (1996) 167.
[24] L.-F. Wang, C.-C. Ou, K.A. Striebel, J.-S. Chen, J. Electrochem. Soc. 150 (7) (2003) 905.
[25] Z. Wang, L. Liu, L. Chen, X. Huang, Solid State Ionics 148 (2002) 335.
[26] Y. Sun, Z. Wang, L. Chen, X. Huang, J. Electrochem. Soc. 150 (10) (2003) A1294.
[27] http://www.xpsdata.com/XI_BE_Lookup_table.pdf.
[28] N. Van Landschoot, C. Kwakernaak, M.W.J. Crajé, W.G. Sloof, E.M. Kelder, J. Schoonman, submitted for publication.
[29] M.M. Thackeray, C.S. Johnson, J.-S. Kim, K.C. Lauzze, J.T. Vaughey, N. Dietz, D. Abraham, S.A. Hackney, W. Zeltner, M.A. Anderson, Electrochem. Com. 5 (2003) 752.
[30] M.J.G. Jak, Dynamic compaction of Li-ion battery components and batteries, Ph.D thesis, Delft University of Technology (1999).
[31] M. Forsyth, D.R. MacFarlane, A.S. Best, J. Adebahr, P. Jacobssen, A.J. Hill, Solid State Ionics 147 (2002) 203.